Single flexible joint impedance

During grasping tasks it is more advantageous to use a joint impedance controller than a joint position controller. Indeed, because the models of the objects are inaccurate, a position controller can lead to large interaction forces. Large forces can damage the fingers or the objects. Consequently, a force control loop is required to *softly* interact with the environment. Several control schemes have been developed that allow to moderate the forces, such as hybrid force control, admittance control or torque control. Based on the practical experience in manipulation of the DLR, a joint impedance controller is selected to provide the compliant behavior. Similar work is proposed in [68], however with experimental results on a very different system (an arm with comparatively large stiffness) as well as limited to the case of a constant stiffness.[1]

In this section, the backstepping design method is applied to a single joint driven by a single motor. Unlike the previous section, the behavior of an impedance controller is targeted. First, the coordinates of the joint model are transformed in order to apply the desired link side control law. The internal dynamics of the motor results in a tracking error of the desired link torque, therefore, the backstepping procedure is applied to ensure that the system is regulated to the desired state while remaining globally stable. In the third section, several simulations are presented in order to obtain a first selection of gains for the experiments. The practical implementation is presented in the last section. A test setup with a single flexible joint and adjustable parameters, such as link mass and joint stiffness, is designed and built for those specify tests.

[1] in [68] the joint stiffness results from the structure stiffness.

15.3.1 Model

Similar to the previous sections, the equations of the simplified system are :

$$\begin{cases} m\ddot{q} &= k(\theta - q) + \tau_{\text{ext}} \\ b\ddot{\theta} &= -k(\theta - q) + \tau_{\text{m}} \end{cases} , \tag{15.51}$$

where $\theta \in \mathbb{R}, q \in \mathbb{R}$ are the motor position and link position. The link inertia and the motor inertia (along the rotation axis) are denoted $m \in \mathbb{R}, b \in \mathbb{R}$. In the linear case, defining $\tau = k(\theta - q)$, and using both equation leads to

$$\ddot{\tau} = -\frac{k(m+b)}{mb}\tau + \frac{k}{b}\tau_{\text{m}} - \frac{k}{m}\tau_{\text{ext}} \ . \tag{15.52}$$

Therefore, θ can be removed from (15.51). Defining the state vector $\boldsymbol{x} \in \mathbb{R}^4$ as $\boldsymbol{x} = [x_1, x_2, x_3, x_4]^T = [q, \dot{q}, \tau, \dot{\tau}]^T$, results in a strict feedback form description

$$\begin{cases} \dot{x}_1 = & x_2 \\ \dot{x}_2 = & m^{-1}(x_3 + \tau_{\text{ext}}) \\ \dot{x}_3 = & x_4 \\ \dot{x}_4 = & \frac{k}{m}\left(-\frac{(m+b)}{m}x_3 + \tau_{\text{m}} - \frac{b}{m}\tau_{\text{ext}}\right) \end{cases} . \tag{15.53}$$

Similar to the example of the previous section, a feedback can be used to cancel most of the terms of the last equation of (15.53).

15.3.2 Controller

The backstepping methodology can be applied in the similar way as in the section 15.2. However, the method does not enforce that the steps are performed one by one if, of course, stability can be established at the end of the step. In the case of an impedance controller, the desired torque is a function of the position and the velocity errors. Recalling that $\bar{x}_3 = x_3 = \tau_{\text{q,des}}$ and using it as a virtual input, the link side controller is designed by selecting $\bar{x}_3$ as

$$\begin{array}{ccc} \tau_{\text{q,des}} & = -K_{\text{p,imp}}q - K_{\text{d,imp}}\dot{q} \\ \Updownarrow & & , \\ \bar{x}_3 & = -K_{\text{p,imp}}x_1 - K_{\text{d,imp}}x_2 \end{array} \tag{15.54}$$

where $(K_{\text{p,imp}}, K_{\text{d,imp}}) \in (\mathbb{R}^{*+})^2$ are the impedance stiffness and damping. The case of a regulation controller to the origin is presented, but the regulation to any other point is obtained by a change of variable. Assuming $\tau_{q,des} = x_3$ can be perfectly generated, the stability is proved using the Lyapunov function, $V_1(q) = \frac{1}{2}\dot{q}^T m\dot{q} + \frac{1}{2}q^T K_{p,imp}q = \frac{1}{2}\dot{x_1}^T m\dot{x_1} + \frac{1}{2}x_1^T K_{p,imp}x_1$. The time derivative of V_1 along the solutions is

$$\begin{aligned} \dot{V}_1(x_1) &= \dot{x}_1^T m\ddot{x}_1 + \dot{x}_1^T K_{\text{p,imp}}x_1 \\ &= x_2^T(-K_{\text{p,imp}}x_1 - K_{\text{d,imp}}x_2 + \tau_{\text{ext}}) + x_2^T K_{\text{p,imp}}x_1 + x_2^T\tau_{\text{ext}} \ , \\ &= -K_{\text{d,imp}}x_2^2 + x_2^T\tau_{\text{ext}} \end{aligned} \tag{15.55}$$

which completes the proof since, in the absence of disturbances $\tau_{\text{ext}} = 0$, thus $\dot{V}_1(x_1) \leq 0$ and $\dot{V}_1(x_1) = 0 \implies x_1 = 0$.

First backstep Since τ_{ext} can not be exactly generated, the error $z_3 = x_3 - \bar{x}_3$ between the reference input and the realized input is introduced. It is interesting to note that the error z_3 is equivalent to the error $\boldsymbol{P}^T \boldsymbol{e}_{\text{f}}$ that was introduced in the cascaded case. The system is expressed in terms of this error as

$$\begin{array}{rcc} \dot{x}_1 = & x_2 & \\ \dot{x}_2 = & m^{-1}(-K_{\text{p,imp}}x_1 - K_{\text{d,imp}}x_2 + z_3 + \tau_{\text{ext}}) & \\ \dot{z}_3 = & x_4 - \dot{\bar{x}}_3 & . \\ \dot{x}_4 = & kb^{-1}(-\dfrac{(m+b)}{m}x_3 + \tau_{\text{m}} - \frac{b}{m}\tau_{\text{ext}}) & \end{array} \tag{15.56}$$

Using $\bar{x}_4 = x_4$ as a virtual input, it is possible to design the link side controller by selecting $\bar{x}_4$ as

$$\bar{x}_4 = -K_3 z_3 + \dot{\bar{x}}_3 - x_2 \ , \tag{15.57}$$

where $K_3 \in \mathbb{R}^{*+}$ is a design parameter. Let $V_2(x_1, x_2, z_3)$ be the Lyapunov function

$$V_2(x_1, x_2, z_3) = \frac{1}{2}\dot{x}_1^T m \dot{x}_1 + \frac{1}{2}x_1^T K_{p,imp} x_1 + \frac{1}{2}z_3^T C_t z_3 \ . \tag{15.58}$$

Thanks to the symmetry of m and $K_{\text{p,imp}}$, the time derivative of V_2 is given by,

$$\dot{V}_2(x_1, x_2, z_3) = \dot{x}_1^T m \dot{x}_2 + x_1 K_{\text{p,imp}} \dot{x}_1 + z_3^T \dot{z}_3 \ . \tag{15.59}$$

Injecting $\dot{x}_2$ and $\dot{z}_3$ from the dynamic equation gives

$$\begin{array}{rcc} \dot{V}_2 & = & x_2^T(-K_{p,imp}x_1 - K_{\text{d,imp}}x_2 + z_3 + \tau_{\text{ext}}) + x_1 K_{\text{p,imp}} x_2 + z_3^T(x_4 - \dot{\bar{x}}_3) \\ & = & x_2^T(-K_{p,imp}x_1 - K_{\text{d,imp}}x_2 + z_3 + \tau_{\text{ext}}) + x_1 K_{\text{p,imp}} x_2 \\ & + & z_3^T(-K_3 z_3 + \dot{\bar{x}}_3 - x_2 - \dot{\bar{x}}_3 - \tau_{\text{ext}}) \\ & = & -x_2^T K_{\text{d,imp}} x_2 - z_3^T K_3 z_3 - z_3^T \tau_{\text{ext}} \end{array} \ , \tag{15.60}$$

which, after invocation of the LaSalle theorem, completes the proof.

Second backstep Since x_4 can not be exactly generated, the error $z_4 = x_4 - \bar{x}_4$ between the reference input and the realized input is introduced and the system is expressed in terms of this error. The system is

$$\begin{array}{rcc} \dot{x}_1 = & x_2 & \\ \dot{x}_2 = & m^{-1}(-K_{p,imp}x_1 - K_{\text{d,imp}}x_2 + z_3 + \tau_{\text{ext}}) & \\ \dot{z}_3 = & -K_3 z_3 - x_2 + z_4 & . \\ \dot{z}_4 = & kb^{-1}(-\dfrac{(m+b)}{m}x_3 + \tau_{\text{m}} - \dfrac{b}{m}\tau_{\text{ext}}) - \dot{\bar{x}}_4 & \end{array} \tag{15.61}$$

Finally, since the motor input τ_{m} is appearing in (15.61) the backstepping ends. The control input τ_{m} is selected as

$$\tau_{\mathrm{m}} = \frac{(m+b)}{m} x_3 + bk^{-1}u + \frac{b}{m}\tau_{\mathrm{ext}} \ , \tag{15.62}$$

$$u = -K_4 z_4 + \dot{\bar{x}}_4 - z_3 \ , \tag{15.63}$$

where $K_4 \in \mathbb{R}^{*+}$ is a design parameter. Let $V_3(x_1, x_2, z_3, z_4)$ be the Lyapunov function

$$V_3(x_1, x_2, z_3, z_4) = \frac{1}{2}\dot{x}_1^T m \dot{x}_1 + \frac{1}{2} x_1^T K_{p,imp} x_1 + \frac{1}{2} z_3^T z_3 + \frac{1}{2} z_4^T z_4 \ . \tag{15.64}$$

The time derivative of V_3 is given by (using the symmetry of m and $K_{\mathrm{p,imp}}$)

$$\dot{V}_3(x_1, x_2, z_3, z_4) = \dot{x}_1^T m \dot{x}_2 + x_1 K_{\mathrm{p,imp}} \dot{x}_1 + z_3^T \dot{z}_3 + z_4^T \dot{z}_4. \tag{15.65}$$

Injecting $\dot{x}_2$, $\dot{z}_3$ and $\dot{z}_4$ from the dynamic equation yields

$$\begin{aligned}
\dot{V}_3 = \ & x_2^T(-K_{p,imp}x_1 - K_{\mathrm{d,imp}}x_2 + z_3 + \tau_{\mathrm{ext}}) + x_1 K_{\mathrm{p,imp}} x_2 + z_3^T(-K_3 z_3 - x_2 + z_4) \\
& + z_4^T(-kb^{-1}(\frac{(m+b)}{m}x_3 + \tau_{\mathrm{m}} - \tfrac{b}{m}\tau_{\mathrm{ext}}) - \dot{\bar{x}}_4) \\
= \ & x_2^T(-K_{p,imp}x_1 - K_{\mathrm{d,imp}}x_2 + z_3) + x_1 K_{\mathrm{p,imp}} x_2 + z_3^T(-K_3 z_3 - x_2 - z_4) \\
& + z_4^T(-K_4 z_4 - z_3) \\
= \ & -x_2^T K_{\mathrm{d,imp}} x_2 - z_3^T K_3 z_3 - z_4^T K_4 z_4 + x_2^T \tau_{\mathrm{ext}}
\end{aligned} \ , \tag{15.66}$$

which completes the proof.

Input expression The input expression is obtained by replacing the expressions of $\bar{x}_3$ and $\bar{x}_4$. It is interesting to note that, using the relations $m\ddot{q} = k(\theta - q) + \tau_{\mathrm{ext}}$ and $mq^{(3)} = k(\dot{\theta} - \dot{q}) + \dot{\tau}_{\mathrm{ext}}$, the derivatives must only be available for the link velocity. The original system was

$$\begin{cases}
\dot{x}_1 = & x_2 \\
\dot{x}_2 = & m^{-1}x_3 \\
\dot{x}_3 = & x_4 \\
\dot{x}_4 = & -kb^{-1}\left(m^{-1}(m+b)x_3 + \tau_m\right) \\
\tau_m = & -m^{-1}(m+b)x_3 - bk^{-1}u \\
u = & -K_4 z_4 + \dot{\bar{x}}_4 - z_3
\end{cases} . \tag{15.67}$$

The virtual inputs are defined as

$$\begin{cases}
\bar{x}_3 = & -K_{p,imp}x_1 - K_{\mathrm{d,imp}}x_2 \\
\bar{x}_4 = & -K_3 z_3 + \dot{\bar{x}}_3 - x_2 \\
\tau_m = & bk^{-1}(-k(mb)^{-1}(m+b)x_3 - K_4 z_4 + \dot{\bar{x}}_4 - z_3)
\end{cases} , \tag{15.68}$$

and the error definitions are

$$\begin{cases}
z_3 = & x_3 - \bar{x}_3 \\
z_4 = & x_4 - \bar{x}_4
\end{cases} . \tag{15.69}$$

Finally, the input expression is

$$\begin{array}{rc} u = & -\frac{b}{k}(K_4K_3K_{\mathrm{p,imp}} + K_{\mathrm{p,imp}})x_1 \\ - & \frac{b}{k}(K_3K_{\mathrm{p,imp}} + K_4(K_3K_{\mathrm{d,imp}} + K_{\mathrm{p,imp}} + 1) + K_{\mathrm{d,imp}})x_2 \\ - & \frac{b}{k}((k\frac{(m+b)}{mb} + K_4(K_3 + K_{\mathrm{d,imp}}m^{-1}) + m^{-1}(K_3K_{\mathrm{d,imp}} + K_{\mathrm{p,imp}}) + 1)x_3 \\ - & \frac{b}{k}(K_4 + K_{\mathrm{d,imp}}m^{-1} + K_3)x_4 \end{array} . \tag{15.70}$$

15.3.3 Simulations

In this section numerical simulations are performed to verify that the designed controller is indeed providing the behavior of an joint impedance controller and that it is stable (naturally limited to numerical experiments). Fig. 15.16 and Fig. 15.17 depict the influence of the controller impedance parameters $K_{\mathrm{p,imp}}$ and $K_{\mathrm{d,imp}}$ on the link position after a step command of 45 degrees (at time $t = 0.5$s) and an external disturbance of 1Nm (at time $t = 1.5$s). In Figure 15.16, it can be seen that the selected joint stiffness of

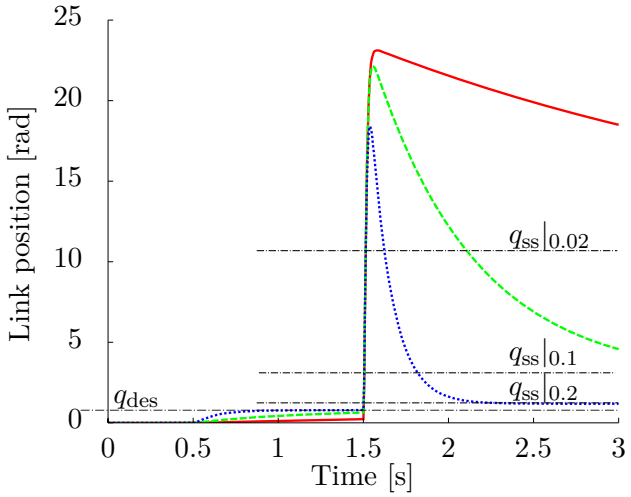

Figure 15.16: Simulation: influence of the stiffness coefficient $K_{\mathrm{p,imp}} \in [0.02, 0.1, 0.5], K_{\mathrm{d,imp}} = 0.05$ on the link side position after a desired position step of 45 degrees (at time $t = 0.5$s) and external disturbance of 0.2Nm (at time $t = 1.5$s).The desired joint position is denoted q_{des} and the steady states are denoted $q_{\mathrm{ss}}|_{0.02}$, $q_{\mathrm{ss}}|_{0.1}$ and $q_{\mathrm{ss}}|_{0.2}$.

the impedance controller leads to the proper steady-state joint deflection. It is interesting to notice that, although the stiffness is modified, the rising times are identical since it is imposed by the motor controller dynamics. In Figure 15.17 the influence of the link damping is noticeable through the increase of the settling time. However, as for the case of the stiffness, the motor dynamics is imposing most of the behavior. Unlike the singular perturbation approach, the system is stable because the motor dynamics are

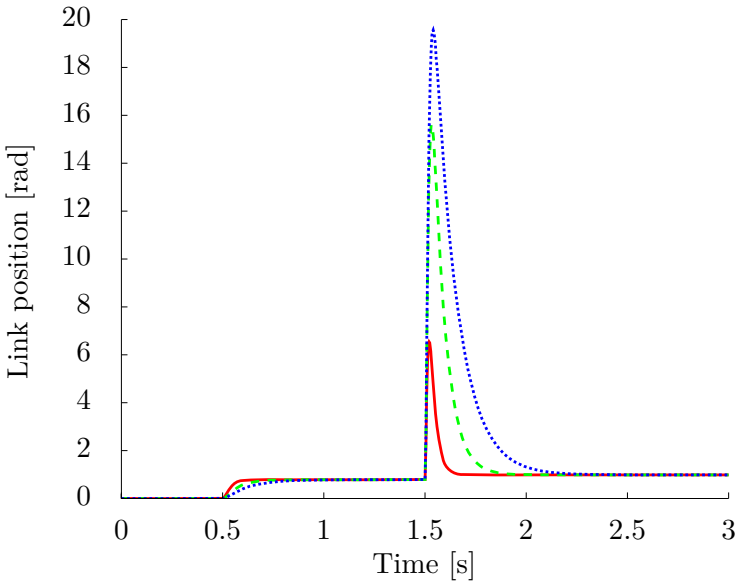

Figure 15.17: Simulation: influence of the damping coefficient $K_{\text{p,imp}} = 1, K_{\text{d,imp}} \in [0.01, 0.05, 0.1]$ on link side position after a desired position step of 45 degrees (at time $t = 0.5$s) and external disturbance of 0.2Nm (at time $t = 1.5$s).

included in the design of the controller and not because of its robustness. In other words, the motor dynamics are not disturbances in the backstepping controller design.

15.3.4 Experiments

Using the same setup as in the previous section, several experiments are performed to verify that the controller behaves as expected with the physical plant. Figure 15.18 shows that the controller successfully moves the link to the desired position and provides an impedance behavior w. r. t. the external load applied (for practical reasons a displacement is imposed to the link and the torque is measured). After applying the displacement to the link, the expected torque should be $\tau = K_{\text{p,imp}}(q - q_0)$ where q (resp. q_0) is the link position (resp. the desired link position). The measured torque is $\tau = 0.579$ Nm for a measured deflection of 0.3 radians and a stiffness of 2 Nm/rad (i. e. an expected torque of $\tau = 0.6$Nm). Although the measured torque is not exactly the expected torque, the behavior is perfectly suited for an interaction between the fingers and the environment.

15.3.5 Conclusion

This section derived an impedance controller for a linear flexible joint driven by a single motor. The controller is designed based on the state controller

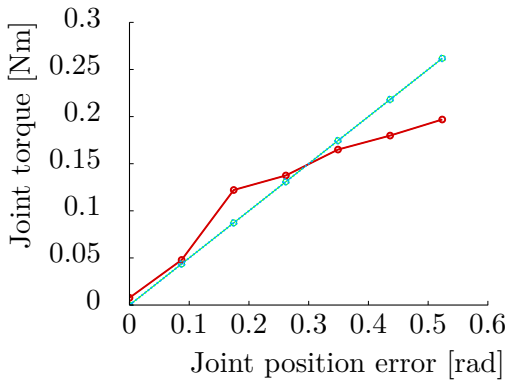

Figure 15.18: Experiment: measured and expected joint torque w. r. t. an increasing joint position error from 0 to 0.5 rad.

of the previous section. It formally requires the measure of the external torque and its derivative. However, it is practically sufficient to neglect the derivative and to estimate the joint torque through the deflection of the spring. Indeed, since the motor position θ and the link position q are measured, the joint torque is obtained as $\tau = k(\theta - q)$ and its derivative $\dot{\tau} = k(\dot{\theta} - \dot{q})$. The usual drawback of the backstepping, that is, the need for high order derivatives, is therefore not a practical issue. Several simulations showed that the controller behaves as an impedance controller. Experiments confirm that the controller performs satisfactorily and reveals to be very robust to disturbances.

15.4 Single flexible joint: impedance non linear stiffness

In the previous sections, the spring stiffness was considered constant. However, in the Hand Arm System, nonlinear springs are used in order to offer the possibility to adjust the joint stiffness. Moreover, the *explosion* of the spring stiffness when reaching its elongation limits creates a natural protection for the end stops of joints. Preliminary experiments on a system with nonlinear springs with the backstepping controller designed for a linear spring showed that the controller is robust to the unmodeled nonlinearities. However, it is possible to include the nonlinear effects directly in the controller to ensure that the stability is achieved without the robustness properties. In this section the backstepping impedance controller for a single flexible joint is modified to include the nonlinear spring characteristic. First, the nonlinearity is introduced in the model. Then, the nonlinear effects are propagated in the controller. The nonlinear effects are only modifying the last backstepping stage. Unsurprisingly, one condition for the stability

proof is that the spring stiffness is strictly positive. Finally, simulations and experiments are performed in order to verify the validity of the controller.

15.4.1 Model

The dynamical model is similar to the previous sections. However, because the spring stiffness is a function of its elongation the system takes the form

$$\begin{array}{ll} m\ddot{q} & = r_q\phi(r_\theta\theta - r_q q) + \tau_{\text{ext}} \\ b\ddot{\theta} & = -r_\theta\phi(r_\theta\theta - r_q q) + \tau_{\text{m}} \end{array} , \tag{15.71}$$

where all quantities are defined as in the linear case. The force generated by the spring is represented by $\phi(r_\theta\theta - r_q q) \in \mathbb{R}$, which is the force depending on the spring elongation. The motor pulley radius and the link pulley radius are denoted $r_\theta \in \mathbb{R}^+$ and $r_q \in \mathbb{R}^+$. In order to simplify the notation, the radii of the motor pulley and the link pulley are considered equal to one. Considering that the spring function is sufficiently smooth on the workspace, defining $\tau = \phi(\theta - q)$ leads to

$$\begin{array}{ll} \dot{\tau} = & \dfrac{\partial\phi}{\partial\theta}(\dot{\theta} - \dot{q}) \\ \ddot{\tau} = & \dfrac{\partial^2\phi}{\partial\theta^2}(\dot{\theta} - \dot{q})^2 + \dfrac{\partial\phi}{\partial\theta}(\ddot{\theta} - \ddot{q}) \end{array} . \tag{15.72}$$

The partial derivative can be taken w. r. t. θ or q because of the symmetry of the function. Using the dynamics to express $\dot{\tau}$ in terms of $q, \dot{q}, \tau$ and $\dot{\tau}$ results in the relation between the spring elongation and the torque, as well as the expression of the torque derivative in terms of the joint torque and the external torque. The expressions are

$$(\dot{\theta} - \dot{q}) = \left(\frac{\partial\phi}{\partial\theta}\right)^{-1}\dot{\tau} , \tag{15.73}$$

and

$$\begin{array}{ll} \ddot{\tau} = & \dfrac{\partial^2\phi}{\partial\theta^2}\left(\left(\dfrac{\partial\phi}{\partial\theta}\right)^{-1}\dot{\tau}\right)^2 + \dfrac{\partial\phi}{\partial\theta}\left(\dfrac{1}{b}\left(-\tau + \tau_{\text{m}}\right) - \dfrac{1}{m}\tau - \dfrac{1}{m}\tau_{\text{ext}}\right) \\ \ddot{\tau} = & \dfrac{\partial^2\phi}{\partial\theta^2}\left(\left(\dfrac{\partial\phi}{\partial\theta}\right)^{-1}\dot{\tau}\right)^2 + \dfrac{\partial\phi}{\partial\theta}\dfrac{1}{b}\left(\tau_{\text{m}} - \dfrac{(b+m)}{m}\tau - \dfrac{b}{m}\tau_{\text{ext}}\right) \end{array} . \tag{15.74}$$

Just as it was done with the linear case, defining the state vector $\boldsymbol{x} \in \mathbb{R}^4$ as $\boldsymbol{x} = [q, \dot{q}, \tau, \dot{\tau}]^T$, results in a strict feedback form description

$$\begin{array}{ll} \dot{x}_1 = & x_2 \\ \dot{x}_2 = & M^{-1}(x_3 + \tau_{\text{ext}}) \\ \dot{x}_3 = & x_4 \\ \dot{x}_4 = & \dfrac{\partial^2\phi}{\partial\theta^2}\left(\left(\dfrac{\partial\phi}{\partial\theta}\right)^{-1}x_4\right)^2 + \dfrac{\partial\phi}{\partial\theta}\dfrac{1}{b}\left(\tau_{\text{m}} - \dfrac{(b+m)}{m}x_3 - \dfrac{b}{m}\tau_{\text{ext}}\right) \end{array} . \tag{15.75}$$

It is important to note that the nonlinear effects are only visible in the last equation of (15.71). None of the partial derivatives is zero since the force characteristic is convex. Therefore, it is possible to feedback linearize the last equation by choosing $\tau_{\mathrm{m}} = \left(\frac{\partial \phi}{\partial \theta}\right)^{-1} b \left(u - \frac{\partial^2 \phi}{\partial \theta^2} \left(\left(\frac{\partial \phi}{\partial \theta}\right)^{-1} x_4 \right)^2 + \frac{(b+m)}{m} x_3 + \frac{b}{m} \tau_{\mathrm{ext}} \right)$.
It yields

$$\begin{array}{rcc} \dot{x}_1 = & x_2 & \\ \dot{x}_2 = & m^{-1} x_3 & \\ \dot{x}_3 = & x_4 & \\ \dot{x}_4 = & u & \end{array} , \tag{15.76}$$

which is similar to the linear case.

15.4.2 Controller

The controller derivation is identical to the case of the linear system until the input expression replacement. The control input u is selected as

$$\tau_{\mathrm{m}} = \left(\frac{\partial \phi}{\partial \theta}\right)^{-1} b \left(u - \frac{\partial^2 \phi}{\partial \theta^2} \left(\left(\frac{\partial \phi}{\partial \theta}\right)^{-1} x_4 \right)^2 \right) + \frac{(b+m)}{bm} x_3 \ , \tag{15.77}$$

with

$$u = -K_4 z_4 + \dot{\bar{x}}_4 - z_3 \ , \tag{15.78}$$

where $K_4 \in \mathbb{R}^{*+}$ is a design parameter. The stability of the plant under the controller is obtained by Lyapunov analysis. Let $V_3(x_1, x_2, z_3, z_4)$ be the Lyapunov function,

$$V_3(x_1, x_2, z_3, z_4) = \frac{1}{2} \dot{x}_1^T m \dot{x}_1 + \frac{1}{2} x_1^T K_{\mathrm{p,imp}} x_1 + \frac{1}{2} z_3^T z_3 + \frac{1}{2} z_4^T z_4 \ . \tag{15.79}$$

The time derivative of V_3 is given by

$$\dot{V}_3(x_1, x_2, z_3, z_4) = \dot{x}_1^T m \dot{x}_2 + x_1 K_{\mathrm{p,imp}} \dot{x}_1 + z_3^T \dot{z}_3 + z_4^T \dot{z}_4 \ . \tag{15.80}$$

Injecting $\dot{x}_2$, $\dot{z}_3$ and $\dot{z}_4$ from the dynamic equation yields

$$\begin{array}{rcc} \dot{V}_3 = & x_2^T(-K_{p,imp} x_1 - K_{d,imp} x_2 + z_3) + x_1 K_{\mathrm{p,imp}} x_2 + z_3^T(-K_3 z_3 - x_2 + z_4) & \\ & + z_4^T((\frac{\partial \phi}{\partial \theta})^{-1} x_4^2 + \frac{\partial^2 \phi}{\partial \theta^2} \frac{1}{b} (\tau_{\mathrm{m}} - \frac{(b+m)}{bm} x_3) - \dot{\bar{x}}_4) & \\ = & x_2^T(-K_{p,imp} x_1 - K_{d,imp} x_2 + z_3) + x_1 K_{\mathrm{p,imp}} x_2 + z_3^T(-K_3 z_3 - x_2 - z_4) & , \\ & + z_4^T(-K_4 z_4 - z_3) & \\ = & -x_2^T K_{d,imp} x_2 - z_3^T K_3 z_3 - z_4^T K_4 z_4 & \end{array} \tag{15.81}$$

which, after invoking LaSalle theorem, completes the proof.

15.4.3 Simulations

In this section numerical simulation are performed to verify that the controller provides an impedance behavior and that it is stable (naturally limited to numerical experiments). For the simulation, a realistic spring characteristic is used and the derivatives are tabulated in a lookup table in order to stay close to the implementation case. Throughout this section, the term *linear* controller refers to the backstepping controller designed for the linear plant, the term *nonlinear* controller refers to the backstepping controller designed for the nonlinear plant. The difference between the linear and the nonlinear controllers is depicted in Figure 15.19. The improvement of the *nonlinear* controller is mainly noticeable in terms of settling time, although a larger overshot is observed. The *nonlinear* components of the controller

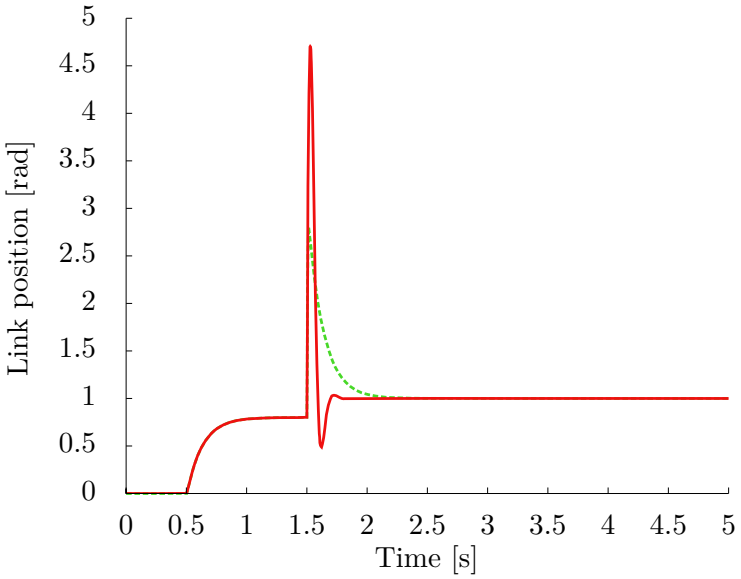

Figure 15.19: Simulation: comparison between the linear backstepping controller and the nonlinear backstepping controller on a nonlinear plant. The solid/red curve depicts the link position under the *nonlinear* controller. The dashed/green curve depicts the link position under the *linear* controller.

have an effect only when the stiffness of the link is far from the nominal stiffness, therefore the difference between the trajectories is not noticeable during the free motion between $t = 0.5s$ and $t = 1.0s$. Indeed, the inertia of the link is low w. r. t. to the joint stiffness thus the link deflection is minimal and the stiffness variation is negligible. A load applied to the link modifies noticeably the stiffness, this effect in depicted in Fig. 15.19 where the stiffness during both experiments is reported. Since a torque peak must be generated to begin the motion, one would expect a change of stiffness at the point denoted by A. However, this change of stiffness is negligible w. r. t.

the change of stiffness imposed by the load. As with most nonlinear control

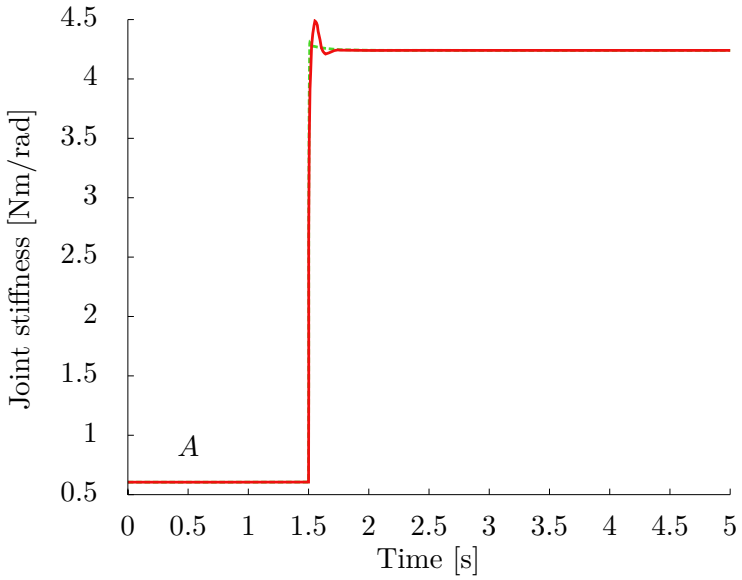

Figure 15.20: Simulation: change of the joint stiffness during the experiment depicted in Fig. 15.19. The solid/red curve depicts the link position under the *nonlinear* controller. The dashed/green curve depicts the link position under the *linear* controller. The stiffness change when accelerating the link (cf. point A, at $t = 0.5s$) is negligible w. r. t. the change of stiffness imposed by the external load (at time $t = 1.5s$).

approaches, the cancellation of the nonlinear terms tends to generate very large control actions. Therefore, a comparison between the *linear* and the *nonlinear* controller, together with an torque input saturation, is reported in Fig. 15.21.

15.4.4 Experiments

Using the same setup as used in the previous section but replacing the linear springs by nonlinear ones, experiments are performed to verify that the controller behaves as expected with the physical plant. Similar to the linear case, the controller successfully moves the link to the desired position and provides an impedance behavior w. r. t. the externally applied load. The link side position and the joint torques trajectories are depicted in Figure 15.22.

15.4.5 Conclusion

This section derived a nonlinear impedance controller for a nonlinear flexible joint driven by a single motor. The equations reveal that the differences between the *linear* backtepping controller and the *nonlinear* backstepping are

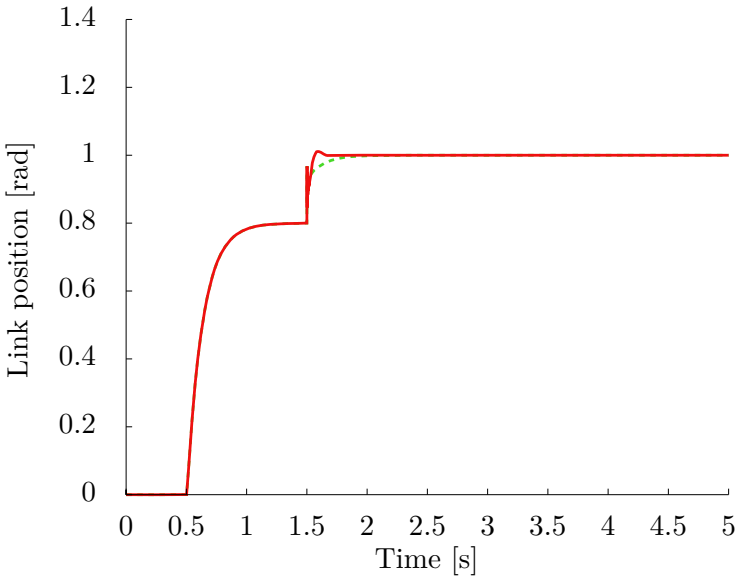

Figure 15.21: Simulation: effect of a motor torque saturation on the controllers. The solid/red curve depicts the link position under the *nonlinear* controller. The dashed/green curve depicts the link position under the *linear* controller. In both cases, a saturation is applied on the motor torque. The difference between the two controller is reduced. Nonetheless, the settling time of the *nonlinear* controller remains shorter.

limited if the input saturation is taken into account. Although the stiffness of the joint is nonlinear, the stiffness of the link only changes significantly when an external load is applied. Simulations and experiments confirm that the controller performs satisfactorily and reveals to be very robust to disturbances. The implementation of this nonlinear backstepping controller requires a stiffness model and its derivatives. It is interesting to note that one condition for the use of the controller is that the stiffness and its first derivative are non zero.

15.5 Antagonistic joint

The previous sections have demonstrated that the backstepping method is able to provide a solid theoretical background as well as excellent practical results. However, the previous cases where limited to the case of a single joint driven by a single motor. As presented in the modeling part, the fingers of the Awiwi Hand are driven by an antagonistic arrangement of tendons thus, it is necessary to extend the backstepping controller to the case of an antagonistic controller.

In this section, the backstepping design method is applied to a single joint driven by a pair of motors. First, the dynamics equations of the system are

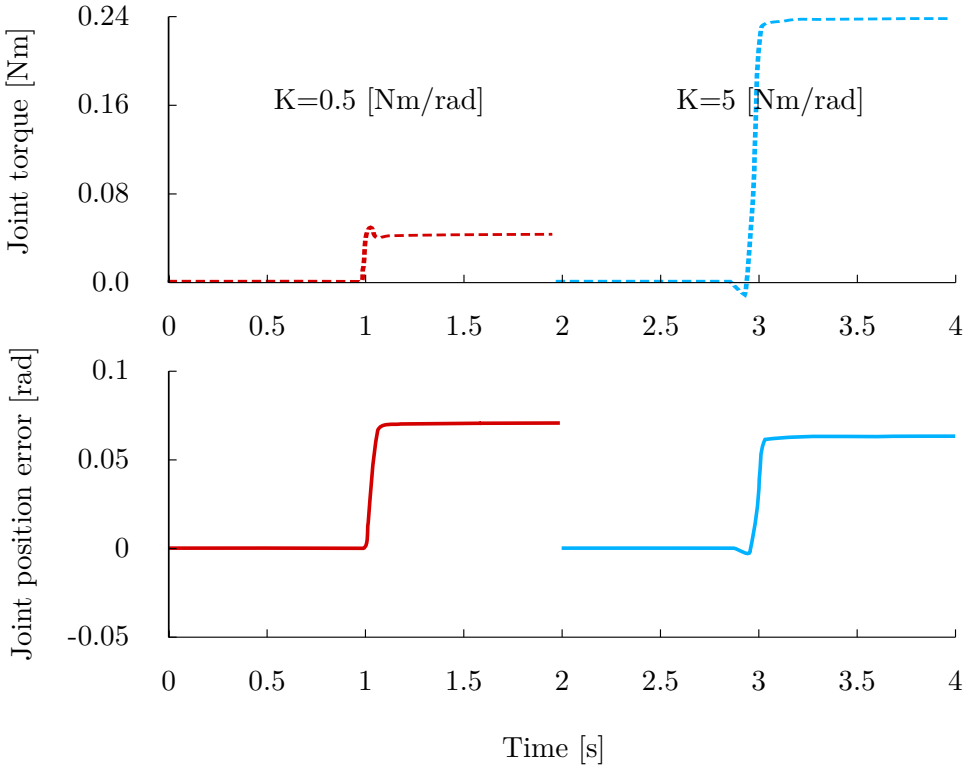

Figure 15.22: Experiment: measured link side position and joint torque after a desired position step of 1.3 rad and external obstacle placed at 0.8 rad. Between 0s and 2s the impedance gain is 0.5Nm/rad (in red). The impedance gain is 5Nm/rad between 2s and 4s (in blue).

derived. The system must be transformed in a strict feedback form to be suited for the backstepping procedure. However, transforming the complete system in such a form would loose the symmetry of the problem. Because it is preferred to keep the system symmetry, it is better to transform it in the strict feedback form by considering that the motors are not *aware* of one another. The desired link torque is shared between the motors and a pretension torque is added in order to maintain the pulling constraints and possibly achieve the desired stiffness. Finally, the backstepping method is applied to the two separated systems with the notations used by [130].

The simulations and experiments are presented in the last part. The main difficulty is to select the numerous gain matrices in order to obtain a satisfactory behavior. The gains have been initially selected to lead to feedback gains for the tendon force error that is close to the cascaded case.

15.5.1 Model

The equations for a linear antagonistic setup are

$$\begin{array}{rcl} m\ddot{q} & = & k(\theta_1 - q) - k(\theta_2 + q) + \tau_{\text{ext}} \\ b_1\ddot{\theta}_1 & = & -k_1(\theta_1 - q) + \tau_{\text{m},1} \\ b_2\ddot{\theta}_2 & = & -k_2(\theta_2 + q) + \tau_{\text{m},2} \end{array}, \tag{15.82}$$

where $(\theta_1, \theta_2) \in \mathbb{R}^2, q \in \mathbb{R}$ are the motor positions and link position. The link inertia and the motor inertia are denoted $m \in \mathbb{R}, b \in \mathbb{R}$. In the following, it is assumed that $b_1 = b_2 = b$ in order to simplify the notations. Defining $\tau_1 = k_1(\theta_1 - q), \tau_2 = k_2(\theta_2 + q)$, and using both equation leads to

$$\begin{array}{rcl} \ddot{\tau}_1 = & \frac{k_1}{m}\left(\frac{(m+b)}{b}\tau_1 + \tau_2 + \frac{m}{b}\tau_{\text{m},1} - \tau_{\text{ext}}\right) \\ \ddot{\tau}_2 = & \frac{k_2}{m}\left(\frac{(m+b)}{b}\tau_2 + \tau_1 + \frac{m}{b}\tau_{\text{m},2} + \tau_{\text{ext}}\right) \end{array}. \tag{15.83}$$

The system (15.83) can be decoupled with

$$\begin{array}{rcl} \tau_{\text{m},1} = & \frac{b}{m}(u - \tau_2) \\ \tau_{\text{m},2} = & \frac{b}{m}(u - \tau_1) \end{array}, \tag{15.84}$$

which yields

$$\begin{array}{rcl} \ddot{\tau}_1 = & \frac{k_1}{m}\left(\frac{(m+b)}{b}\tau_1 + u_1 - \tau_{\text{ext}}\right) \\ \ddot{\tau}_2 = & \frac{k_2}{m}\left(\frac{(m+b)}{b}\tau_2 + u_2 + \tau_{\text{ext}}\right) \end{array}. \tag{15.85}$$

Therefore, both motors can be treated independently. The following treats the case of θ_1. Defining the state vector $\boldsymbol{x} \in \mathbb{R}^4$ as $\boldsymbol{x} = [x_1, x_2, x_3, x_4]^T = [q, \dot{q}, \tau_1, \dot{\tau}_1]^T$, results in a strict feedback form description

$$\begin{array}{rcl} \dot{x}_1 = & x_2 \\ \dot{x}_2 = & m^{-1}(x_3 + \tau_{\text{ext}}) \\ \dot{x}_3 = & x_4 \\ \dot{x}_4 = & \frac{k_1}{m}\left(\frac{(m+b)}{b}x_3 + u_1 - \tau_{\text{ext}}\right) \end{array}. \tag{15.86}$$

Since an impedance behavior of the link side is wished, we have

$$\tau_{\text{q,des}} = \tau_1 - \tau_2 = -K_{\text{p,imp}}q - K_{\text{d,imp}}\dot{q} \tag{15.87}$$

However, because two motors are acting one the joint, they exists many combinations of motor torques that generate the desired joint torque. The choice

$$\begin{array}{rcl} \bar{\tau}_1 = & \tau_{1,\text{offset}} + \frac{1}{2}\tau_{\text{q,des}} \\ \bar{\tau}_2 = & \tau_{2,\text{offset}} - \frac{1}{2}\tau_{\text{q,des}} \end{array}, \tag{15.88}$$

where $\bar{\tau}_1$ and $\bar{\tau}_2$ denote the desired torque to be produced by each motor, is a choice that symmetrically shares the torque.

First backstep

Because the two motors have been decoupled it is possible to treat the problem as a set of independent differential systems. Therefore, all quantities are scalars. Let $V_2(\boldsymbol{x})$, be the Lyapunov function

$$V_2(\boldsymbol{x}) = \frac{1}{2}mx_2^2 + \frac{1}{2}K_{\text{p,imp}}x_1^2 + \frac{1}{2}e_{\text{t}}^T C_{\text{t}} e_{\text{t}} \ , \tag{15.89}$$

where $C_{\text{t}} \in \mathbb{R}$ and $K_{\text{p,imp}} \in \mathbb{R}$ are two positive scalars. The torque tracking error $e_{\text{t}} \in \mathbb{R}$ is defined as

$$e_t = \tau_1 - \bar{\tau}_1 = x_3 - \bar{x}_3 \ . \tag{15.90}$$

The time derivative of V_2 is given by

$$\dot{V}_2(q) = \dot{q}^T M\ddot{q} + qK_{p,imp}\dot{q} + e_t^T C_t \dot{e}_t \ . \tag{15.91}$$

Injecting $\ddot{q}$ from the dynamic equation gives

$$\dot{V}_2(q) = \dot{q}^T(-K_{p,imp}q - K_{d,imp}\dot{q} + e_t) + qK_{p,imp}\dot{q} + e_t^T C_t \dot{e}_t \ , \tag{15.92}$$

further simplified in

$$\dot{V}_2(q) = -\dot{q}^T K_{d,imp}\dot{q} + \dot{q}e_t + e_t^T C_t \dot{e}_t \ . \tag{15.93}$$

It is possible to cancel the positive term $\dot{q}e_t$ by choosing a suitable $\dot{e}_t$, however the cancellation must account for an new tracking error e_s. Inserting the error gives

$$\dot{e}_t = \dot{e}_{t,des} + e_s \tag{15.94}$$

$$\dot{e}_{t,des} = -C_t^{-1}(\dot{q} - K_t e_t) \ , \tag{15.95}$$

and leads to

$$\dot{V}_2(q) = -\dot{q}^T K_{d,imp}\dot{q} - e_t^T K_t e_t + e_t^T C_t e_s \ . \tag{15.96}$$

Second backstep

To eliminate $e_t^T C_t e_s$ from $\dot{V}_2$ one needs to perform a second time the procedure. Let V_3 be a Lyapunov function including the missing term

$$V_3(q) = \frac{1}{2}\dot{q}^T M\dot{q} + \frac{1}{2}q^T K_{p,imp}q + \frac{1}{2}e_t^T C_t e_t + \frac{1}{2}e_s^T C_s e_s \tag{15.97}$$

The time derivative is

$$\dot{V}_3(q) = \dot{q}^T M\ddot{q} + q^T K_{p,imp}\dot{q} + e_t^T C_t \dot{e}_t + e_s^T C_s \dot{e}_s \tag{15.98}$$

Replacing $\ddot{q}$ and $\dot{e}_t$

$$\dot{V}_3(q) = \dot{q}^T(-K_{p,imp}q - K_{d,imp}\dot{q} + e_t) + q^T K_{p,imp}\dot{q} + e_t^T C_t(-C_t^{-1}(\dot{q} - K_t e_t) + e_s) + e_s^T C_s \dot{e}_s \tag{15.99}$$

Simplified in

$$\dot{V}_3(q) = -K_{d,imp}\dot{q}^2 - e_t^T K_t e_t + e_t^T C_t e_s + e_s^T C_s \dot{e}_s \tag{15.100}$$

It is possible to cancel the positive term $e_t^T C_t e_s$ by choosing a suitable $\dot{e}_s$

$$\dot{e}_s = \ddot{\tau} - \ddot{\tau}_d - \ddot{e}_{t,des} \tag{15.101}$$

Once the torque dynamic equations are placed back in the Lyapunov V_3

$$\dot{V}_3(q) = -K_{d,imp}\dot{q}^2 - e_t^T K_t e_t + e_t^T C_t e_s + e_s^T C_s(\ddot{\tau} - \ddot{\tau}_d - \ddot{e}_{t,des}) \tag{15.102}$$

Substituting $\ddot{\tau}$

$$\dot{V}_3(q) = -K_{d,imp}\dot{q}^2 - e_t^T K_t e_t + e_t^T C_t e_s + e_s^T C_s(KB^{-1}(\tau_m - B\ddot{q} - \tau) - \ddot{\tau}_d - \ddot{e}_{t,des}) \tag{15.103}$$

The control law is selected as

$$\tau_m = B\ddot{q} + \tau + BK^{-1}(\ddot{\tau}_d + \ddot{e}_{t,des} - C_s^{-1}C_t e_t - C_s^{-1}K_s e_s) \ , \tag{15.104}$$

which gives the Lyapunov derivative $\dot{V}_3$

$$\dot{V}_3(q) = -\dot{q}^T K_{d,imp}\dot{q} - e_t^T K_t e_t - e_s^T C_s e_s \ . \tag{15.105}$$

Input expression

The input expression is obtained by recursively replacing the expression of the errors. The final expression is given by

$$\tau_m = B\ddot{q} + \tau + BK^{-1}(\ddot{\tau}_d - C_t^{-1}(q^{(3)} - K_t(\ddot{\tau} - \ddot{\tau}_d)) - C_s^{-1}C_t(\tau - \tau_d) - C_s^{-1}K_s(C_t^{-1}\ddot{q} + (1 - C_t^{-1}K_t)(\dot{\tau} - \dot{\tau}_d))) \ . \tag{15.106}$$

15.5.2 Simulations

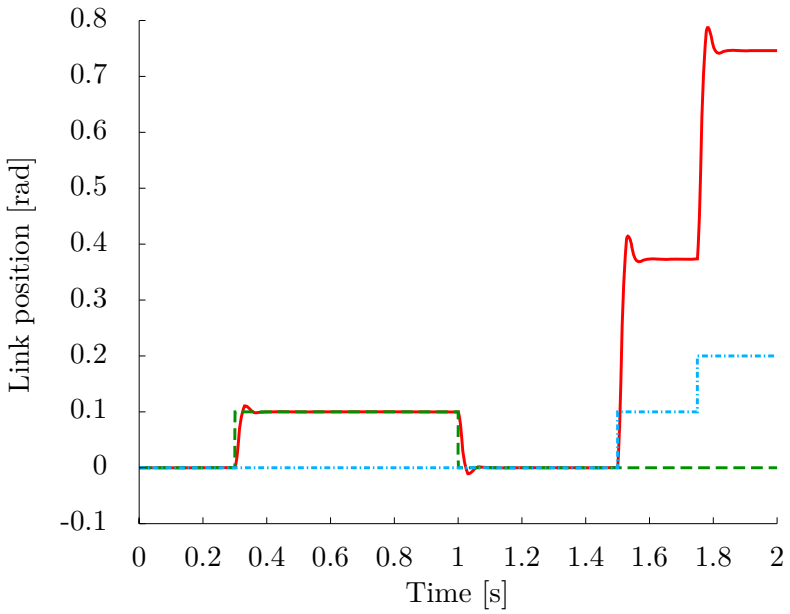

Figure 15.23: The plot depicts the simulated link position, in red/solid and the desired link position, in green/dashed along with the external joint torque, in light blue/dashed-dotted.

In figure 15.23, the results of the backstepping controller simulation are reported. In a first time, a position step is commanded and the link successfully moves to the desired position. In a second time, the desired position is maintained constant and an external torque is applied. As depicted the link is deflected according to the impedance control law.

15.5.3 Experiments

The performance of the backsptepping controller has been tested on a single finger and the results were compared with the ones of the cascaded controller. The finger used is a finger with bearings and steel cables.

Step response and sinus tracking results The figure 15.24 shows the step response for the PIP joint. The step response is an important indicator of the speed and the accuracy of the system which is particularly useful for rapid motions. Figure 15.25 reports the tracking of a sinus, which is a good representation of the motion used in a grasp approach phase.

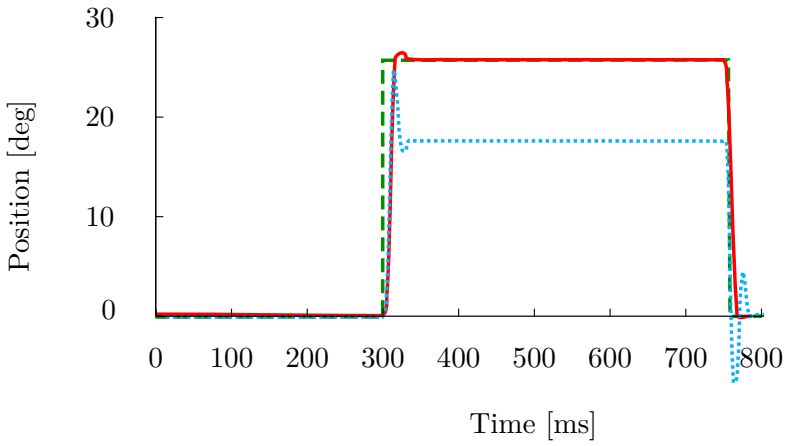

Figure 15.24: Step response for the PIP joint. Pretension forces were set to $f_{int} = 10N$. The green/dashed curve depict the desired position. The solid/red one represents the response with the backstepping controller. The light blue/dotted one shows the response with the cascaded controller.

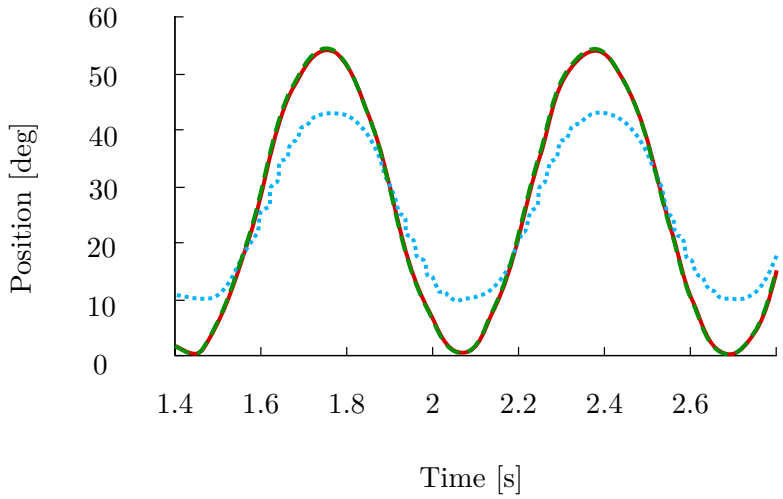

Figure 15.25: Sinus tracking for the PIP joint. The pretension forces are set to $f_{pre} = 15N$. The green/dashed curve depicts the desired position. The red/solid one depicts the response with the backstepping controller. The light blue/dotted one represents the response with the cascaded controller. The vibrations of the light blue/dotted signal are caused by the stick-slip effect.

The backstepping controller shows accuracy and speed that are in the required range for grasping and throwing objects. The cascaded controller is inaccurate because the maximum impedance gain $\boldsymbol{K}_{\mathrm{p,imp}}$ that can be selected without amplifying the sensor noise is significantly lower than in

the case of the backsteppping controller.

Gain diagram A comparison of the gain diagram of the singular perturbation controller of the previous chapter and the antagonistic backstepping is depicted in Fig. 15.26. For each experiment two sets of gains are depicted. One set corresponds to the gain obtained for the positive half sinus and the other one is associated with the negative sinus wave. The backstepping controller results in a unit gain over a longer range of frequency than the singular perturbation controller. It is interesting to note that the singular perturbation controller systematically underestimates the actual link displacement and yields an incorrect sinus amplitude. The singular perturbation controller using the link side position was unable to produce a stiffness comparable to the backstepping controller, therefore, the experiment has been performed with the link position using only the motor positions. It is the reason why the amplitude is incorrect.

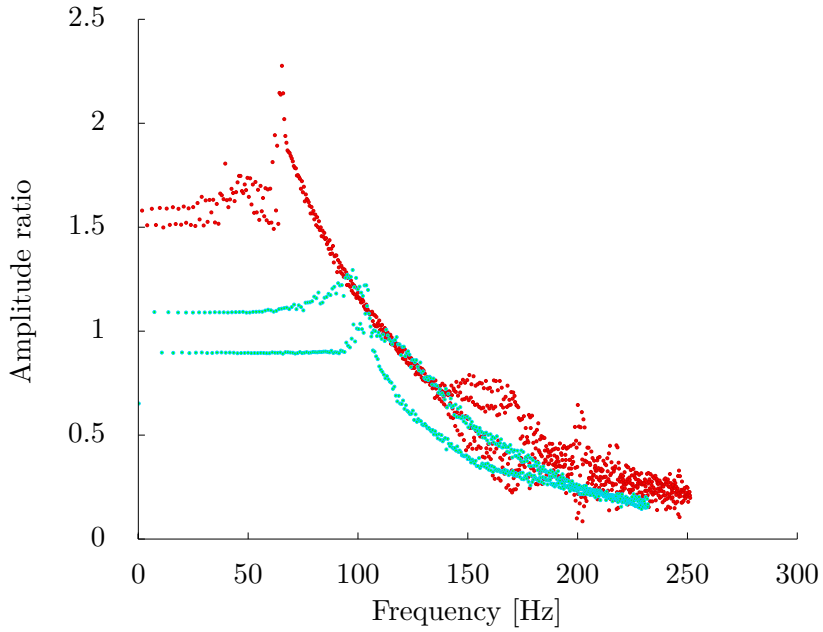

Figure 15.26: Gain diagram for the PIP join controlled by the backstepping controller (indicated by light blue dots) and the singular perturbation controller (red dots). The pretension was set to $f_{pre} = 20N$ for both experiments.

Validation of the impedance behavior The influence of $\boldsymbol{K}_{\mathrm{p,imp}}$ has been tested for the backstepping controller. It is verified experimentally that the antagonistic backstepping controller design is resulting in the expected impedance behavior. More specifically, the stiffness component is verified.

The experiment consists in imposing a joint deflection with a mechanical fixture and compare the torque generated by the measured tendon forces and the desired joint stiffness. The results are reported in Figure 15.27.

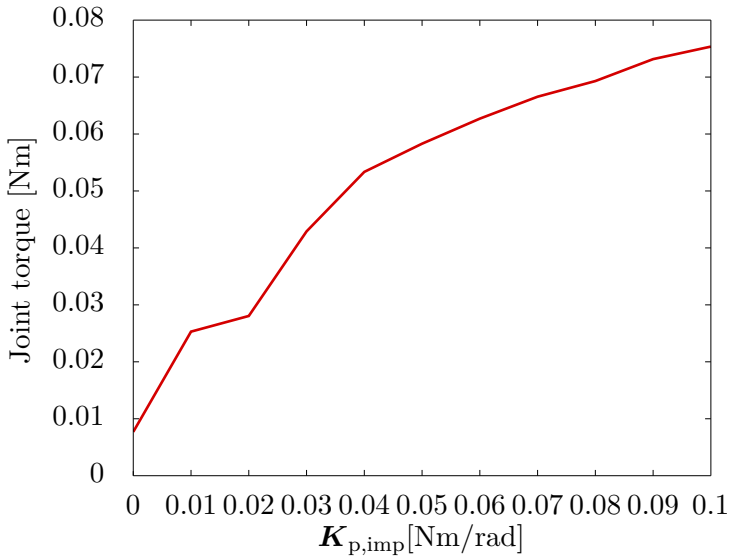

Figure 15.27: The curve depicts the joint torque generated by the tendon forces depending on the desired impedance stiffness. A position error of the joint was imposed externally by a mechanical fixture.

15.5.4 Conclusion

In this section, the backstepping method has been extended to the case of an antagonistic actuation. The extension, based on a very simple sharing of the desired joint torque, allows to derived two symmetric controllers. Dealing with both motor independently allows to avoid dealing with a system of order six. Moreover, because the symmetry is conserved, the pretension of the tendon is naturally introduced as a shifting of the desired working point. The simulations and the experimental results both confirmed that the method sucessfully provides an impedance behavior.

15.6 Conclusion

In this chapter the backstepping method has been applied. It is a nonlinear control method adapted to problems that can be written in a strict feedback form. The chapter first introduced the method on an academic example. Then, the method was applied to a state controller. The state controller was then modified to produce an impedance behavior. Simulations and experiments confirmed the performance of the controller. The controller was

modified to account for the nonlinear spring behavior and it has been shown that only minor modifications are required. The saturation of the motor torque limits the advantage of using a controller that accounts for the plant nonlinearities. Finally, the backstepping controller was extended to the case of the antagonistic actuation. Simulations and experiments confirm that the method is successfully providing a link side impedance behavior. The method is superior to the cascaded case in the sense that it allows to reach higher impedance stiffness and thus better link side positioning accuracy.

It is important to note that the choice of the gains to obtain the desired behavior is a challenge. In the presented experiments and simulations the gains have initially been selected to be close to the gains of the cascaded control. The gains were then tuned manually, which is a slow and imprecise method, until the behavior was satisfactory. This tuning method is very tedious for a full hand. Therefore, a systematic method to select and adjust the gains is investigated in the next chapter.